Published in final edited form as:
Magn Reson Med. 2009 April ; 61(4): 981–988. doi:10.1002/mrm.21851.

Balanced Multi-point Displacement Encoding for DENSE MRI

Xiaodong Zhong, M.S.[1], **Patrick A. Helm, Ph.D.**[2], and **Frederick H. Epstein, Ph.D.**[1,2]
[1]Biomedical Engineering, University of Virginia, Charlottesville, Virginia, United States

[2]Radiology, University of Virginia, Charlottesville, Virginia, United States

Abstract

Displacement encoding with stimulated echoes (DENSE) is a quantitative imaging technique that encodes tissue displacement in the phase of the acquired signal. Various DENSE sequences have encoded displacement using methods analogous to the simple multi-point methods of phase contrast (PC) MRI. We developed general n-dimension balanced multi-point encoding for DENSE. Using these methods, phase noise variance decreased experimentally by 73.7%, 65.6%, and 61.9% compared to simple methods, which closely matched the theoretical decreases of 75%, 66.7%, and 62.5% for 1D, 2D, and 3D encoding, respectively. Phase noise covariances decreased by 99.2% and 99.3% for balanced 2D and 3D encoding, consistent with the zero-covariance prediction. The direction bias inherent to the simple methods was decreased to almost zero using balanced methods. Reduced phase noise and improved displacement and strain maps using balanced methods were visually observed in phantom and volunteer images. Balanced multi-point encoding can also be applied to PC MRI.

Keywords

MRI; DENSE; displacement encoding; velocity encoding; tagging

Introduction

Displacement-encoded imaging with stimulated echoes (DENSE) is a quantitative tissue motion imaging technique which encodes tissue displacement in the phase of the stimulated echo (1-5). In addition to encoded displacement, the phase of the stimulated echo is influenced by off-resonance effects such as B0 inhomogeneity. If phase shifts from sources other than the encoded displacement are not accounted for, they lead to errors in the measured tissue motion (6). Therefore, instead of the absolute phase, multiple measurements are required to obtain the desired phase shifts that precisely represent tissue motion (1-5).

To date, various multi-dimensional DENSE sequences have encoded displacement in two or three orthogonal directions, and have acquired an additional phase reference image without displacement encoding for background correction (1-5). This encoding strategy is precisely analogous to the simple multi-point method for velocity-encoded phase contrast (PC) (7). However, this strategy does not provide optimal noise properties or symmetry. A balanced four-point encoding strategy with improved noise variance and symmetry has been previously described for 3D velocity-encoded PC, but not for the general n-dimensional case (7).

Please send all correspondence to: Frederick H. Epstein, Ph.D., Radiology Department, University of Virginia, Box 801339, Charlottesville, VA 22908, Phone: 434-982-0563, Fax: 434-924-9435, Email: fredepstein@virginia.edu. Address for reprint requests: University of Virginia, Radiology Department, Room 1186, MR4 Building, 409 Lane Rd., Charlottesville, VA 22908.

We developed a general balanced multi-point strategy for n-dimensional displacement encoding and processing of DENSE MR data (8). The balanced multi-point methods were compared to simple multi-point methods in one, two, and three dimensions both theoretically and experimentally. The theoretical comparison employed an extension of previous methods for analyzing noise variance (7,9). The experimental results were obtained by implementing both the simple and balanced methods and imaging a stationary water phantom and a human volunteer.

Theory

Encoding and Decoding

As described previously (5,10,11), the transverse magnetization that forms a DENSE image, $M_{xy}(\vec{r},t)$, can be written as Eq. [1]:

$$M_{xy}(\vec{r},t)=M\sin(\alpha)e^{-t/T1}e^{-j(\vec{k}\bullet\Delta\vec{r}+\Delta\theta_b)} \quad [1]$$

where M is the longitudinal magnetization prior to application of the excitation pulse, α is the flip angle of the excitation pulse, $\vec{k}$ is the spatial frequency vector imparted to the transverse magnetization by the displacement encoding gradients, $\Delta\vec{r}$ is the tissue displacement that occurs during the mixing time t, and $\Delta\theta_b$ is the background phase due to off-resonance effects. Assuming N scans are performed to extract the displacements in the orthogonal directions (x-, y-, and/or z), and the same displacement encoding frequency k_e is used to encode all orthogonal directions, the displacement encoding of these scans can be described in matrix form as Eq. [2]:

$$\begin{bmatrix}\varphi_1\\ \vdots\\ \varphi_N\end{bmatrix}=\left[\begin{array}{ccc|c}W_{1x} & W_{1y} & W_{1z} & 1\\ \vdots & \vdots & \vdots & \vdots\\ W_{Nx} & W_{Ny} & W_{Nz} & 1\end{array}\right]\begin{bmatrix}k_e\Delta x\\ k_e\Delta y\\ \frac{k_e\Delta z}{\Delta\theta_b}\end{bmatrix} \quad [2]$$

In Eq. [2], φ_i is the phase of the stimulated echo image of the ith scan. $W_{i,dir}$ is the weighting value of the encoded displacement in the *dir* direction, which composes the encoding matrix. The column on the right side of the encoding matrix contains all 1's, since the weighting of the background phase cannot be manipulated. Δx through Δz correspond to the displacements in the x through z directions, respectively.

In order to solve the measured displacements and background phase, Eq. [2] can be denoted as Eq. [3] for simplicity:

$$\Phi=WD \quad [3]$$

Then the displacements and background phase can be solved by Eq. [4]:

$$D=(W^TW)^{-1}W^T\Phi \quad [4]$$

where the superscript *T* denotes the matrix transpose operation, and the superscript -1 denotes the matrix inverse operation. This process, which extracts the displacements and the background phase from the phase of the encoded stimulated echo images, is called decoding.

Simple Multi-Point vs. Balanced Multi-Point Encoding

The most straightforward way to spatially encode the n-dimensional displacement measurement is the simple encoding method. In this method, one scan is performed to provide a phase reference image, and other scans encode for displacement in the orthogonal *x*-, *y*-, and/or *z* directions. The simple two-, three- and four-point encoding methods for 1D, 2D and 3D displacement encoding are illustrated by Fig. 1a, 1c and 1e, respectively, and can be expressed by Eqs. [5], [7] and [9] in Table 1, respectively. The corresponding decoding matrices are given by Eqs. [6], [8] and [10] in Table 1.

For the balanced encoding methods, the directions of the encoding vectors are designed to be evenly distributed in space, and the encoding matrices are obtained by calculating the vertex coordinates of the encoding vectors. For 1D DENSE imaging, balanced two-point encoding is similar to the two-point method in 1D velocity-encoded PC imaging: two scans are acquired with displacement encoding of opposite polarities along one direction, as shown in Fig. 1b and described by Eq. [11] in Table 1. In the 2D case, the encoding directions of the balanced three-point method must be along the three circumradii of an equilateral triangle with center located at the origin, as shown in Fig. 1d. One instance of the balanced three-point method is expressed by Eq. [13] in Table 1, where the weighting coefficients of the first scan are calculated by putting one circumradius on the *x* axis, and the weighting coefficients of the other scans are obtained by calculating the remaining vertex coordinates of this equilateral triangle. In order to achieve an equivalent displacement weighting, the composite displacement-encoding vector is set to be a unit vector, as for the simple three-point method. The same concept can be extended to the 3D case. The encoding directions of the balanced four-point method can be determined by the four circumradii of a regular tetrahedron as shown in Fig. 1f. Eq. [15] gives an example encoding matrix for the balanced four-point method with the weighting values in the three spatial directions scaled to make a unit composite vector. The corresponding balanced two-, three- and four-point decoding matrices are given by Eqs. [12], [14] and [16] in Table 1.

Noise Variance

Assuming the noise is equal and uncorrelated in each scan, the noise variance in each phase image is given by Eq. [17]:

$$\sigma_{\varphi}^{2}=\sigma^{2}/|S|^{2} \qquad [17]$$

where σ^2 is the noise variance in the complex image, and $|S|$ is the magnitude of the signal in the voxel of interest (9). As for velocity-encoded PC (7), and as shown in the appendix, the noise variances of the displacement-encoded phase images for each method are calculated and listed in the theoretical values column in Table 2. The phase noise variance values of the balanced methods are expected to be only 25%, 33.3% and 37.5% of those of the simple methods for 1D, 2D and 3D DENSE, respectively. Using the derivation in the appendix, the covariance between any two directions for each method can be calculated. The corresponding values are listed in the theoretical values column in Table 3. Unlike the simple methods, which have non-zero phase noise covariance between any two directions, the balanced methods have independent phase noise (zero noise covariance between any two directions) since all scans contribute to all displacement measurements equally.

Non-integer Scaling of Phase Angle

Some practical issues occur when implementing the balanced multi-point encoding methods for online DENSE data reconstruction. To increase the sensitivity of DENSE, the displacement encoding frequency is generally set to a value such that some phase wrapping occurs for the largest tissue displacement. Phase unwrapping is then performed during displacement analysis of the phase-reconstructed images. Because the values in the decoding matrix in Eq. [12] are not integers, unless phase unwrapping is performed prior to decoding, the non-integer scaling of phase angles will introduce phase errors. However, phase unwrapping is usually performed offline after decoding because the phase unwrapping algorithm is non-deterministic and can fail. Thus, this step is usually implemented in post processing, so that manual intervention may be used to correct algorithm failures. To avoid subsequent errors in phase unwrapping while still performing online DENSE reconstruction of phase images, only integer scaling can be performed during decoding, and the residual scaling factor is applied later, after phase unwrapping, when calculating displacement. This approach is provided by Eq. [18] for the 1D case such that:

$$\begin{bmatrix} 2k_e\Delta x \\ 2\Delta E \end{bmatrix} = \begin{bmatrix} 1 & -1 \\ 1 & 1 \end{bmatrix} \begin{bmatrix} \varphi_1 \\ \varphi_2 \end{bmatrix} \quad [18]$$

Similarly, Eqs. [19] and [20] are for the 2D and 3D cases, respectively:

$$\begin{bmatrix} 3k_e\Delta x \\ \sqrt{3}k_e\Delta y \\ 3\Delta E \end{bmatrix} = \begin{bmatrix} 2 & -1 & -1 \\ 0 & 1 & -1 \\ 1 & 1 & 1 \end{bmatrix} \begin{bmatrix} \varphi_1 \\ \varphi_2 \\ \varphi_3 \end{bmatrix} \quad [19]$$

$$\begin{bmatrix} 4\sqrt{3}k_e\Delta x/3 \\ 4\sqrt{3}k_e\Delta y/3 \\ 4\sqrt{3}k_e\Delta z/3 \\ 4\Delta E \end{bmatrix} = \begin{bmatrix} -1 & 1 & 1 & -1 \\ -1 & 1 & -1 & 1 \\ -1 & -1 & 1 & 1 \\ 1 & 1 & 1 & 1 \end{bmatrix} \begin{bmatrix} \varphi_1 \\ \varphi_2 \\ \varphi_3 \\ \varphi_4 \end{bmatrix} \quad [20]$$

Interestingly, the displacement-weighting values in the *x*- and *y*-encoded phase images ($3k_e\Delta x$ and $\sqrt{3}k_e\Delta y$) of the online reconstructed results for the balanced three-point encoding method are not the same (Eq. [19]). Therefore, the *x*-encoded phase images have larger phase values than the *y*-encoded phase images after online decoding. This difference is accounted for later offline by application of the residual scaling factor.

In addition, notice the differences of the left side of the online decoding equations between the balanced and simple methods (Eq. [18] versus [6], [19] versus [8], and [20] versus [10]). The online reconstructed phase images of the balanced methods are expected to have more phase wrapping than those of the simple methods because of the residual scaling factors.

Materials and Methods

Phantom Experiments

The noise variances of the balanced and simple encoding methods were measured on a stationary water phantom for DENSE imaging with 1D, 2D and 3D displacement encoding. All studies were performed on a 1.5T MRI system (Avanto, Siemens Medical Solutions,

Germany). An ECG-gated spiral cine DENSE pulse sequence (12) was modified to perform either simple or balanced displacement encoding, as well as phase cycling (5,13,14) for artifact suppression. The imaging parameters included pixel size = 2.5 × 2.5 mm^2, slice thickness = 2.5 mm, flip angle = 20°, TR = 18 ms, TE = 1.8 ms, number of interleaves = 6, temporal resolution = 36 ms, and frames = 16. Both encoding methods used displacement encoding frequency k_e = 0.1 cycles/mm (15). Through-plane dephasing with the frequency of k_d = 0.08 cycles/mm was used for improved artifact suppression for the cases of 1D and 2D displacement encoding (11).

Phase noise was obtained by measuring the phase values in a region of interest (ROI) encompassing a large area of the phantom in phase-reconstructed images after decoding and applying the residual scaling factor if necessary (no phase unwrapping is needed for the stationary phantom data). The phase noise variance of the balanced encoding methods and the simple encoding methods were calculated for the *x*, *y* and *z* directions, respectively, and the average phase noise variance values were then computed. The absolute value of the phase noise covariance between every two directions was computed for the three- and four-point cases for both the simple and balanced methods. The ratios of the balanced to the simple methods were also calculated.

Displacement was directly extracted from the phase images for each direction, and then combined into an overall displacement vector. The direction bias of the displacement error vectors associated with the 2D and 3D methods was quantified using principal component analysis on the displacement error vectors. Briefly, a dyadic tensor, *F*, was formed from the displacement error vectors $\vec{v}_i$ as in Eq. [21]:

$$F = \sum_{i=1}^{M} \left(\vec{v}_i\right)^T \cdot \left(\vec{v}_i\right) \quad [21]$$

where *M* is the total number of the displacement error vectors. The principal eigenvectors and eigenvalues of the dyadic tensor represent the direction and magnitude of the highest variance of the displacement error vectors. We quantified the overall bias *E* of each encoding strategy as Eq. [22]:

$$E = \sqrt{\frac{3}{2}} \frac{\sqrt{\left(\lambda_1 - \bar{\lambda}\right)^2 + \left(\lambda_2 - \bar{\lambda}\right)^2 + \left(\lambda_3 - \bar{\lambda}\right)^2}}{\sqrt{\left(\lambda_1^2 + \lambda_2^2 + \lambda_3^2\right)}} \quad [22]$$

where λ_i are the eigenvalues and $\bar{\lambda}$ is the trace of the dyadic tensor. This metric is similar to fractional anisotropy commonly used in diffusion tensor imaging. It has a value of 0 for the perfectly isotropic case (no direction bias) and a value of 1 when a single direction bias exists.

Volunteer Imaging

After informed consent was obtained, one healthy volunteer was scanned using the same 1.5T scanner. The human study was performed in accordance with protocols approved by our institutional review board. The same cine DENSE sequence used for the phantom experiments was used to image the left ventricle (LV) of the volunteer. The imaging parameters included pixel size = 2.4 × 2.4 mm^2, slice thickness = 5 mm, flip angle = 20°, TR

= 15 ms, TE = 1.2 ms, number of interleaves = 6, temporal resolution = 30 ms, and frames = 24. Both encoding methods used displacement encoding frequency k_e = 0.06 cycles/mm to provide a good balance between sensitivity to displacement, intravoxel dephasing, and phase wrapping (15). Complementary spatial modulation of magnetization (CSPAMM) with through-plane dephasing frequency k_d = 0.08 cycles/mm was used for artifact suppression during breath-holding for the cases of 1D and 2D displacement encoding (11). With the other parameters unchanged, both the simple and balanced encoding methods were used.

Phase-reconstructed DENSE images were calculated online, and subsequent displacement and strain analysis of these data were performed offline using MATLAB (The Mathworks Inc., Natick, MA, United States) as described previously (15).

Results

Phase-reconstructed DENSE images of the stationary phantom visually demonstrate the reduced phase noise of the balanced three-point method (Fig. 2b) compared to the simple three-point method (Fig. 2a). The reduced phase noise is readily apparent in zoomed 2D displacement maps from the marked region of interest in the phantom, which show smaller displacement magnitudes using the balanced three-point method (Fig. 2d) compared to the simple three-point method (Fig. 2c).

The phase noise variance values measured from the phantom data are listed in Table 2. Compared to the simple methods, the balanced methods decreased the measured phase noise variance by 73.7%, 65.6%, and 61.9% for 1D, 2D, and 3D displacement encoding, respectively, which closely match the predicted theoretical values of 75%, 66.7%, and 62.5%. The absolute value of the phase noise covariance between every two directions was calculated for the three- and four-point cases for both the simple and balanced methods. The ratios of the balanced to the simple methods were then calculated, and listed in Table 3. As observed, the balanced methods eliminate the phase noise covariance between any two directions by 99.2% and 99.3% for the 2D and 3D cases, respectively, compared to the simple methods. These results are consistent with the theoretical zero-covariance prediction.

Histograms and scatter plots of the displacement error vectors of both the balanced and simple methods from the stationary phantom data are shown in Fig. 3. Using the balanced encoding methods, smaller displacement errors were achieved. Moreover, direction bias was predicted and observed for the simple three- and four-point methods, while the balanced multi-point encoding methods display greatly reduced direction bias. For three-point encoding, the overall biases of the simple and balanced methods are 0.525973 and 0.085938, respectively. For four-point encoding, the overall biases of the simple and balanced methods were 0.708840 and 0.068900, respectively.

Reduced phase noise is also observed in the unwrapped phase images of the volunteer data for the balanced three-point method (Fig. 4b) compared to the simple three-point method (Fig. 4a). This leads to reduced noise in the circumferential strain map for the balanced three-point method (Fig. 4d) compared to the simple three-point method (Fig. 4c).

Discussion

The advantages of balanced multi-point encoding include three main aspects. First, balanced methods provide equivalent phase noise in all directions. Second, for a fixed encoding frequency k_e, balanced methods provide increased phase signal-to-noise ratio (SNR). In velocity-encoded PC, the velocity encoding strength can be increased essentially without penalty and can therefore be readily adjusted to provide similar phase SNR and wrapping for the simple and balanced methods. However, this is not the case in DENSE. For DENSE

there is an SNR penalty associated with increasing values of k_e due to intravoxel dephasing (15). Thus, for DENSE the balanced and simple methods should be compared at equivalent k_e values. For this reason, the balanced method may be particularly advantageous for DENSE. Last, the concept of balanced multi-point encoding can be extended for signal averaging. More scans, not necessarily multiples of the minimum number of scans, can be used with the balanced encoding method to further increase the phase SNR. For example, for 2D displacement encoding, rather than the minimum of 3 scans, 4 balanced scans could be used. The encoding matrix could be obtained by calculating the vertex coordinates of a square. Therefore, if there is more imaging time available, but not enough for one more complete average, the balanced method could fully utilize the extra time. Even if multiples of the minimum number of scans are used, the balanced encoding methods are still preferred because of better performance than averaging. For example, to measure 2D displacement, the phase noise variance of the balanced six-point encoding method is only one-third of the phase noise variance of the simple three-point encoding method with two signal averages.

Perhaps the only limitation of the balanced multi-point encoding strategy is more phase wrapping in the online reconstructed images compared to the simple multi-point method when online reconstruction and integer scaling are used. However, if all the DENSE data are reconstructed offline, then phase unwrapping can be performed before the linear combination of the phase values of the scans, and there would be no more phase wrapping for the balanced method because non-integer scaling can be directly applied.

In this study, the encoding matrices of the balanced methods were generated using typical geometrical shapes. Theoretically any rotation and/or scaling of these geometrical shapes provide a variant of the encoding matrices.

The balanced four-point encoding method in the previous velocity-encoded PC imaging study (7) used a Hadamard matrix to generate the encoding matrix. This method is a special case of the general algorithm described here and has the composite displacement-encoding vector scaled by a factor of $\sqrt{3}$ compared to a unit vector. Some other multi-point displacement encoding strategies assign the directions of the encoding vectors only on the Cartesian axes (16,17). For 2D imaging, the noise variance values of the decoded phase in the *x* and *y* directions, provided by the three-point encoding method ((Y,Z), (-Y,Z) and (X,Z)) in (16), are 75% and 25% of the noise variance values of the simple three-point encoding method, respectively. For 3D imaging, the noise variance values of the decoded phase in the *x*, *y* and *z* directions, provided by the four-point encoding method ((Y,Z), (-Y,Z), (X,Z) and (X,-Z)) in (17), are 75%, 25% and 25% of the noise variance values of the simple four-point encoding method, respectively. Although the phase noise variance values in some directions are lower than those of the balanced methods, the phase noise variances in the *x* direction are much higher than those of the balanced methods. Moreover, the encoding methods in (16,17) have unequal phase noise variance values in different directions and non-zero noise covariance values between any two directions.

In summary, the balanced multi-point encoding method provides reduced phase noise variance for a given displacement encoding frequency, and eliminates the direction bias in phase noise. The only disadvantage of the balanced method is when online DENSE reconstruction is required, the intermediate online reconstructed phase may have increased phase wrapping. The algorithms for the balanced methods in this study can be applied generally to encode in n-dimensions for DENSE acquisitions, and can also be applied to velocity-encoded PC imaging. In DENSE, because signal loss due to intravoxel dephasing increases with increasing k_e, there is an inherent advantage in decreasing the noise variance for a given value of k_e.

Acknowledgments

This study was supported in part by NIH grant RO1 EB 001763 and Siemens Medical Solutions.

Appendix

Theoretical Calculation of Phase Noise Variance for Each Direction for DENSE Data

The variance of a linear sum of multiple variables is given by Eq. [23]:

$$\mathrm{var}\left(\sum_{i=1}^{N} a_i X_i\right)=\sum_{i=1}^{N} a_i^2 \mathrm{var}(X_i)+2\sum_{i=1}^{N}\sum_{j=1}^{N} a_i a_j \mathrm{cov}(X_i, X_j) \quad [23]$$

where X_i is a random variable, var(X_i) is its variance, and cov(X_i, X_j) is the covariance between X_i and X_j.

As an example, the phase noise variance of both balanced and simple three-point methods are calculated in this section. For the simple three-point method, the displacement-encoded phase values in the x and y directions can be rewritten as Eq. [24]:

$$\begin{cases} k_e \Delta x = -\varphi_1 + \varphi_2 \\ k_e \Delta y = -\varphi_1 + \varphi_3 \end{cases} \quad [24]$$

Given equal and uncorrelated noise variance in the phase image of each scan by Eq. [17], the phase noise variance of the displacement-encoded phase values in the x and y directions can be calculated as Eq. [25] (note cov(φ_1,φ_2) = 0):

$$\begin{cases} \sigma^2_{k_e \Delta x} = 2\sigma^2_{\varphi} \\ \sigma^2_{k_e \Delta y} = 2\sigma^2_{\varphi} \end{cases} \quad [25]$$

For the balanced three-point method, the displacement-encoded phase values in the x and y directions can be rewritten as Eq. [26]:

$$\begin{cases} k_e \Delta x = \frac{2}{3}\varphi_1 - \frac{1}{3}\varphi_2 - \frac{1}{3}\varphi_3 \\ k_e \Delta y = \frac{\sqrt{3}}{3}\varphi_2 - \frac{\sqrt{3}}{3}\varphi_3 \end{cases} \quad [26]$$

The phase noise variance in the x and y directions can be calculated in Eq. [27]:

$$\begin{cases} \sigma^2_{k_e \Delta x} = \frac{4}{9}\sigma^2_1 + \frac{1}{9}\sigma^2_2 + \frac{1}{9}\sigma^2_3 = \frac{2}{3}\sigma^2_{\varphi} \\ \sigma^2_{k_e \Delta y} = \frac{1}{3}\sigma^2_2 + \frac{1}{3}\sigma^2_3 = \frac{2}{3}\sigma^2_{\varphi} \end{cases} \quad [27]$$

Theoretical Calculation of Phase Noise Covariance between Two Directions for DENSE Data

For the case of two random variables, Eq. [23] can be simplified as Eq. [28]:

$$\mathrm{var}(a_1X_1+a_2X_2)=a_1^2\mathrm{var}(X_1)+a_2^2\mathrm{var}(X_2)+2a_1a_2\,\mathrm{cov}(X_1,X_2) \quad [28]$$

Therefore, the covariance between $k_e\Delta x$ and $k_e\Delta y$ can be calculated by Eq. [29]:

$$\mathrm{var}(k_e\Delta x,k_e\Delta y)=\frac{\mathrm{var}(k_e\Delta x+k_e\Delta y)-\mathrm{var}(k_e\Delta x)-\mathrm{var}(k_e\Delta y)}{2} \quad [29]$$

For the simple three-point method, the covariance between the x and y directions can be calculated as Eq. [30]:

$$\mathrm{var}(k_e\Delta x,k_e\Delta y)=\frac{\mathrm{var}(-2\varphi_1+\varphi_2+\varphi_3)-2\sigma_\varphi^2-2\sigma_\varphi^2}{2}=\sigma_\varphi^2 \quad [30]$$

For the balanced three-point method, the covariance between the x and y directions can be calculated as Eq. [31]:

$$\mathrm{var}(k_e\Delta x,k_e\Delta y)=\frac{\mathrm{var}(\frac{2}{3}\varphi_1+\frac{\sqrt{3}-1}{3}\varphi_2-\frac{\sqrt{3}+1}{3}\varphi_3)-\frac{2}{3}\sigma_\varphi^2-\frac{2}{3}\sigma_\varphi^2}{2}=0 \quad [31]$$

References

1. Aletras AH, Ding S, Balaban RS, Wen H. DENSE: Displacement encoding with stimulated echoes in cardiac functional MRI. J Magn Reson. 1999; 137:247–252. [PubMed: 10053155]
2. Aletras AH, Balaban RS, Wen H. High-resolution strain analysis of the human heart with fast-DENSE. J Magn Reson. 1999; 140:41–57. [PubMed: 10479548]
3. Aletras AH, Wen H. Mixed echo train acquisition displacement encoding with stimulated echoes: An optimized DENSE method for in vivo functional imaging of the human heart. Magn Reson Med. 2001; 46:523–534. [PubMed: 11550245]
4. Gilson WD, Yang Z, French BA, Epstein FH. Complementary displacement-encoded MRI for contrast-enhanced infarct detection and quantification of myocardial function in mice. Magn Reson Med. 2004; 51:744–752. [PubMed: 15065247]
5. Kim D, Gilson WD, Kramer CM, Epstein FH. Myocardial tissue tracking with two-dimensional cine displacement-encoded MRI — development and initial evaluation. Radiology. 2004; 230:862–871. [PubMed: 14739307]
6. Zhong, X.; Spottiswoode, BS.; Epstein, FH. Improved efficiency in cine DENSE using low resolution phase reference images. Proceedings of the 14th Annual Meeting of ISMRM; Seattle, WA, USA. 2006. p. 3583
7. Pelc NJ, Bernstein MA, Shimakawa A, Glover GH. Encoding strategies for three-direction phase-contrast MR imaging of flow. J Magn Reson Imaging. 1991; 1:405–413. [PubMed: 1790362]

8. Zhong, X.; Helm, PA.; Young, A.; Kirton, R.; Epstein, FH. Improved DENSE MRI using balanced multi-point displacement encoding. Proceedings of the 15th Annual Meeting of ISMRM; Berlin, Germany. 2007. p. 965

9. Conturo TE, Smith GD. Signal-to-noise in phase angle reconstruction: dynamic range extension using phase reference offsets. Magn Reson Med. 1990; 15:420–437. [PubMed: 2233221]

10. Epstein FH, Gilson WD. Displacement-encoded cardiac MRI using cosine and sine modulation to eliminate (CANSEL) artifact-generating echoes. Magn Reson Med. 2004; 52:774–781. [PubMed: 15389939]

11. Zhong X, Spottiswoode BS, Cowart EA, Gilson WD, Epstein FH. Selective suppression of artifact-generating echoes in cine DENSE using through-plane dephasing. Magn Reson Med. 2006; 56:1126–1131. [PubMed: 17036303]

12. Meyer, CH. Spiral echo-planar imaging. In: Schmitt, F.; Stehling, MK.; Turner, R., editors. Echo-planar imaging: theory, technique, and application. Berlin and Heidelberg: Springer Verlag; 1998. p. 633-658.

13. Callot V, Bennett E, Decking UKM, Balaban RS, Wen H. In vivo study of microcirculation in canine myocardium using the IVIM method. Magn Reson Med. 2003; 50:531–540. [PubMed: 12939761]

14. Tsao, J.; Laurent, D. N-SPAMM for efficient displacement-encoded acquisition in myocardial tagging. Proceedings of the 13th Annual Meeting of ISMRM; Miami, FL, USA. 2005. p. 273

15. Spottiswoode BS, Zhong X, Hess AT, Kramer CM, Meintjes EM, Mayosi BM, Epstein FH. Tracking myocardial motion from cine DENSE images using spatiotemporal phase unwrapping and temporal fitting. IEEE Trans Med Imaging. 2007; 26:15–30. [PubMed: 17243581]

16. Bennett, E.; Spottiswoode, BS.; Lorenz, CH.; Wen, H. Optimal combination of phase cycling and gradient spoiling in DENSE displacement mapping. Proceedings of the 14th Annual Meeting of ISMRM; Seattle, WA, USA. 2006. p. 1649

17. Wen H, Marsolo KA, Bennett EE, Kutten KS, Lewis RP, Lipps DB, Epstein ND, Plehn JF, Croisille P. Adaptive postprocessing techniques for myocardial tissue tracking with displacement-encoded MR imaging. Radiology. 2008; 246:229–240. [PubMed: 18096537]

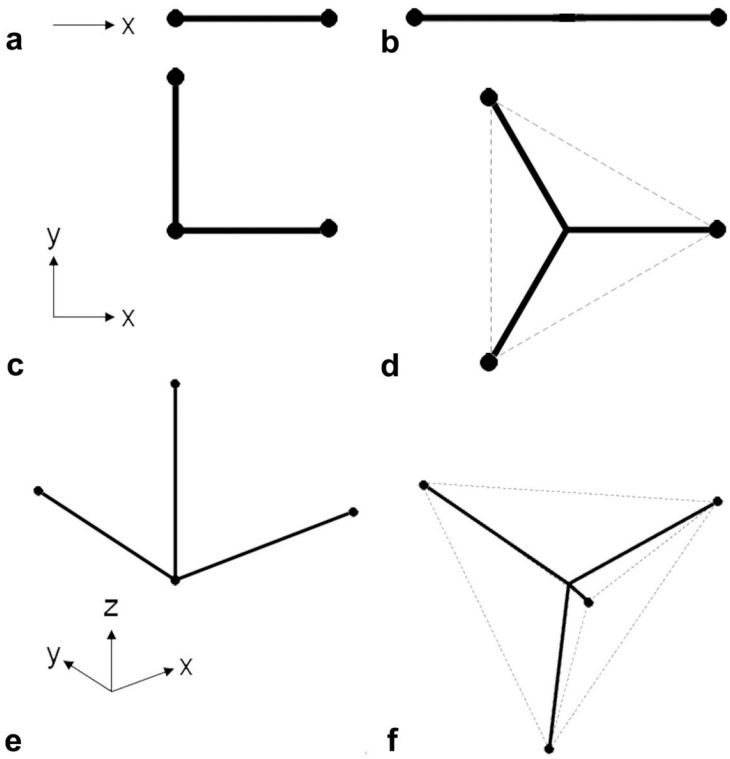

Fig. 1.

Geometric shapes used to generate the weighting and directions of the encoding vectors for both simple (a, c, e) and balanced (b, d, f) multi-point displacement-encoding strategies. The top row (a, b): two-point encoding in 1D space. The middle row (c, d): three-point encoding in 2D space. The bottom row (e, f): four-point encoding in 3D space. The bars with the dots at the end indicate the encoding vectors. For the simple encoding strategies, an additional phase reference image without displacement encoding is also acquired, as indicated by the dot at the origin.

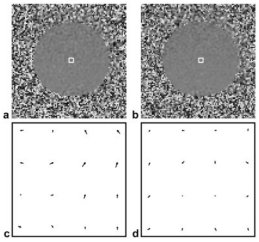

Fig. 2.
Example DENSE phase images and displacement maps of the stationary phantom for both simple (a, c) and balanced (b, d) three-point displacement-encoding strategies. The top row (a, b): phase images representing displacement in the *y* direction. The bottom row (c, d): the pixel-by-pixel 2D displacement maps of the area marked by the square boxes shown in (a) and (b).

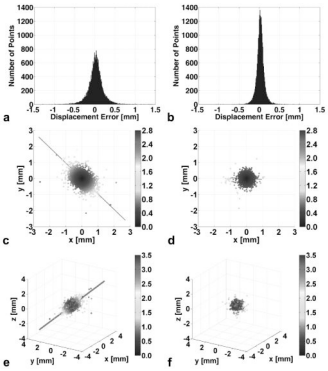

Fig. 3.

Measured displacement error plots for simple (a, c, e) and balanced (b, d, f) multi-point displacement encoding from a stationary water phantom. Displacement error histograms for the simple (a) and balanced (b) two-point encoding methods. Two-dimensional displacement error scatter plots for the simple (c) and balanced (d) three-point encoding methods. Three-dimensional displacement error scatter plots for the simple (e) and balanced (f) four-point encoding methods. The gray level of the points in (c-f) represents the magnitude of the displacement error vector. The unit is in mm. The straight lines in (c-f) indicate the principal eigenvectors of the dyadic tensors, whose lengths correspond to the eigenvalues scaled by a factor of 1/350 for improved visualization. The eigenvectors quantify the direction bias of the encoding strategies.

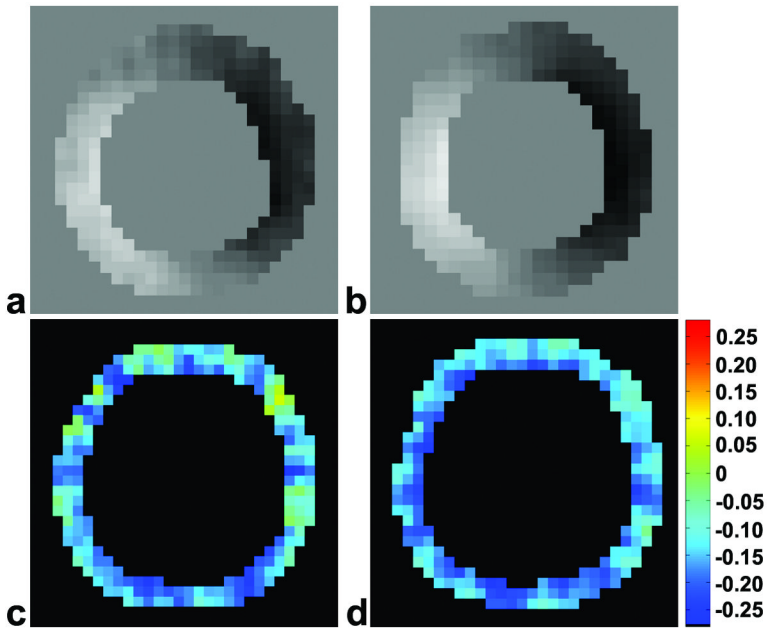

Fig. 4.

Example short-axis DENSE phase images and circumferential strain (Ecc) maps of the LV of a healthy volunteer for both simple (a, c) and balanced (b, d) three-point displacement-encoding. The top row (a, b): end-systolic phase images representing displacement in the *x* direction. The bottom row (c, d): 2D end-systolic Ecc maps.

Table 1

Equations of the simple and balanced multi-point displacement encoding strategies

		Encoding		Decoding	
Simple	Two-point	$\begin{bmatrix}\varphi_1\\ \varphi_2\end{bmatrix}=\begin{bmatrix}0 & 1\\ 1 & 1\end{bmatrix}\begin{bmatrix}k_e\Delta x\\ \Delta\theta_b\end{bmatrix}$	Eq. [5]	$\begin{bmatrix}k_e\Delta x\\ \Delta\theta_b\end{bmatrix}=\begin{bmatrix}-1 & 1\\ 1 & 0\end{bmatrix}\begin{bmatrix}\varphi_1\\ \varphi_2\end{bmatrix}$	Eq. [6]
	Three-point	$\begin{bmatrix}\varphi_1\\ \varphi_2\\ \varphi_3\end{bmatrix}=\begin{bmatrix}0 & 0 & 1\\ 1 & 0 & 1\\ 0 & 1 & 1\end{bmatrix}\begin{bmatrix}k_e\Delta x\\ k_e\Delta y\\ \Delta\theta_b\end{bmatrix}$	Eq. [7]	$\begin{bmatrix}k_e\Delta x\\ k_e\Delta y\\ \Delta\theta_b\end{bmatrix}=\begin{bmatrix}-1 & 1 & 0\\ -1 & 0 & 1\\ 1 & 0 & 0\end{bmatrix}\begin{bmatrix}\varphi_1\\ \varphi_2\\ \varphi_3\end{bmatrix}$	Eq. [8]
	Four-point	$\begin{bmatrix}\varphi_1\\ \varphi_2\\ \varphi_3\\ \varphi_4\end{bmatrix}=\begin{bmatrix}0 & 0 & 0 & 1\\ 1 & 0 & 0 & 1\\ 0 & 1 & 0 & 1\\ 0 & 0 & 1 & 1\end{bmatrix}\begin{bmatrix}k_e\Delta x\\ k_e\Delta y\\ k_e\Delta z\\ \Delta\theta_b\end{bmatrix}$	Eq. [9]	$\begin{bmatrix}k_e\Delta x\\ k_e\Delta y\\ k_e\Delta z\\ \Delta\theta_b\end{bmatrix}=\begin{bmatrix}-1 & 1 & 0 & 0\\ -1 & 0 & 1 & 0\\ -1 & 0 & 0 & 1\\ 1 & 0 & 0 & 0\end{bmatrix}\begin{bmatrix}\varphi_1\\ \varphi_2\\ \varphi_3\\ \varphi_4\end{bmatrix}$	Eq. [10]
Balanced	Two-point	$\begin{bmatrix}\varphi_1\\ \varphi_2\end{bmatrix}=\begin{bmatrix}1 & 1\\ -1 & 1\end{bmatrix}\begin{bmatrix}k_e\Delta x\\ \Delta\theta_b\end{bmatrix}$	Eq. [11]	$\begin{bmatrix}k_e\Delta x\\ \Delta\theta_b\end{bmatrix}=\begin{bmatrix}1/2 & -1/2\\ 1/2 & 1/2\end{bmatrix}\begin{bmatrix}\varphi_1\\ \varphi_2\end{bmatrix}$	Eq. [12]
	Three-point	$\begin{bmatrix}\varphi_1\\ \varphi_2\\ \varphi_3\end{bmatrix}=\begin{bmatrix}1 & 0 & 1\\ -1/2 & \sqrt{3}/2 & 1\\ -1/2 & -\sqrt{3}/2 & 1\end{bmatrix}\begin{bmatrix}k_e\Delta x\\ k_e\Delta y\\ \Delta\theta_b\end{bmatrix}$	Eq. [13]	$\begin{bmatrix}k_e\Delta x\\ k_e\Delta y\\ \Delta\theta_b\end{bmatrix}=\begin{bmatrix}2/3 & -1/3 & -1/3\\ 0 & \sqrt{3}/3 & -\sqrt{3}/3\\ 1/3 & 1/3 & 1/3\end{bmatrix}\begin{bmatrix}\varphi_1\\ \varphi_2\\ \varphi_3\end{bmatrix}$	Eq. [14]

	Encoding		Decoding	
Four-point	$\begin{bmatrix}\varphi_1\\ \varphi_2\\ \varphi_3\\ \varphi_4\end{bmatrix} = \begin{bmatrix}-\sqrt{3}/3 & -\sqrt{3}/3 & -\sqrt{3}/3 & 1\\ \sqrt{3}/3 & \sqrt{3}/3 & -\sqrt{3}/3 & 1\\ \sqrt{3}/3 & -\sqrt{3}/3 & \sqrt{3}/3 & 1\\ -\sqrt{3}/3 & \sqrt{3}/3 & \sqrt{3}/3 & 1\end{bmatrix}\begin{bmatrix}k_e\Delta x\\ k_e\Delta y\\ k_e\Delta z\\ \Delta\theta_b\end{bmatrix}$	Eq. [15]	$\begin{bmatrix}k_e\Delta x\\ k_e\Delta y\\ k_e\Delta z\\ \Delta\theta_b\end{bmatrix} = \begin{bmatrix}-\sqrt{3}/4 & \sqrt{3}/4 & \sqrt{3}/4 & -\sqrt{3}/4\\ -\sqrt{3}/4 & \sqrt{3}/4 & -\sqrt{3}/4 & \sqrt{3}/4\\ -\sqrt{3}/4 & -\sqrt{3}/4 & \sqrt{3}/4 & \sqrt{3}/4\\ 1/4 & 1/4 & 1/4 & 1/4\end{bmatrix}\begin{bmatrix}\varphi_1\\ \varphi_2\\ \varphi_3\\ \varphi_4\end{bmatrix}$	Eq. [16]

Table 2

Phase noise variance and ratio values of balanced encoding strategies versus simple encoding strategies

		Theoretical values	Experimental values			
			σ_x^2	σ_y^2	σ_z^2	$\overline{\sigma^2}$
Two-point	**Balanced**	$\sigma_\varphi^2/2$	0.02371	–	–	0.02371
	Simple	$2\sigma_\varphi^2$	0.09018	–	–	0.09018
	Bal/Sim	25%	26.3%	–	–	26.3%
Three-point	**Balanced**	$2\sigma_\varphi^2/3$	0.03325	0.03061	–	0.03193
	Simple	$2\sigma_\varphi^2$	0.09341	0.09196	–	0.09269
	Bal/Sim	33.3%	35.6%	33.3%	–	34.4%
Four-point	**Balanced**	$3\sigma_\varphi^2/4$	0.03339	0.03692	0.03690	0.03574
	Simple	$2\sigma_\varphi^2$	0.09450	0.09502	0.09157	0.09370
	Bal/Sim	37.5%	35.3%	38.9%	40.3%	38.1%

Table 3

The absolute value of phase noise covariance between every two directions for balanced encoding strategies and simple encoding strategies and the corresponding ratios

		Theoretical values	Experimental values			
			$\lvert\mathrm{cov}(x, y)\rvert$	$\lvert\mathrm{cov}(x, z)\rvert$	$\lvert\mathrm{cov}(y, z)\rvert$	$\overline{\mathrm{cov}}$
Three-point	Balanced	0	0.00033	–	–	0.00033
	Simple	σ_φ^2	0.04361	–	–	0.04361
	Bal/Sim	0	0.8%	–	–	0.8%
Four-point	Balanced	0	0.00044	0.00014	0.00034	0.00031
	Simple	σ_φ^2	0.04644	0.04753	0.04609	0.04669
	Bal/Sim	0	0.9%	0.3%	0.7%	0.7%